

Multifunctional Hydrogel Dressing That Carries Three Antibiotics Simultaneously and Enables Real-Time Ultrasound Bacterial Colony Detection

Yao-Wei Yeh, Chih-Chung Huang, Wen-Shuo Kuo, Tzu-Lung Liao, Tsung-Lin Tsai, and Ping-Ching Wu*



Cite This: *ACS Omega* 2023, 8, 10278–10287



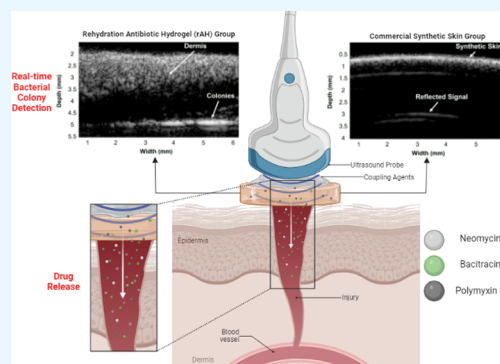
Read Online

ACCESS |

Metrics & More

Article Recommendations

ABSTRACT: We have developed a multifunctional hydrogel that can carry three synergistic antibiotics commonly used in clinical practice. This hydrogel was discovered to have drug encapsulation efficiencies of 94% for neomycin, 97% for bacitracin, and 88% for polymyxin B. Drug release data indicated that the release profiles of these three antibiotics were different. A swelling test demonstrated that the hydrogel absorbed liquid after the release of its antibiotics until it became saturated, which occurred within 48 h. Moreover, this hydrogel exhibited excellent antibacterial effects against *Escherichia coli* and *Pseudomonas aeruginosa* and biocompatibility; it can thus protect a wound from microbial invasion. When the alginate hydrogel is used to cover a wound, the wound can be checked for colonization at any time using ultrasound imaging; this can thus enable the prevention of wound biofilm formation in the early stages of infection. We evaluated the hydrogel against commercially available wound dressings and discovered that these wound dressings did not have the aforementioned desirable features. In conclusion, our multifunctional hydrogel can carry three types of antibiotics simultaneously and is a suitable medium through which an ultrasound can be performed to detect the growth of colonies in wounds. The hydrogel is expected to make a valuable contribution to the prevention of wound infections in the future.



1. INTRODUCTION

Advancements in science and technology have enabled the development of various materials that can be used as wound dressings, such as sponges,¹ hydrogels,² hydrocolloids,³ and films and membranes.^{4,5} Among these materials, hydrogels, which are cross-linked polymer networks, can contain up to 96% water. Hydrogels in sheet or liquid gel form are used to cover a wound or are injected into it, respectively. Owing to their network architecture, hydrogels can potentially be loaded with a drug, which is subsequently released in a controlled manner; they can also absorb tissue fluid, which is a promising strategy for treating necrotic wounds.⁶ Calcium alginate wound dressings have been extensively used in recent years because of their ability to promote postoperative hemostasis and the development of healthy granular tissues.^{7,8} The calcium ions present in the dressing are exchanged for sodium ions present in the serum and wound exudate, triggering the calcium signal transduction pathway through ion exchange and even inducing genes that prompt resting cells to re-enter the cell cycle.⁹

Bacterial contamination of skin wounds is responsible for high morbidity and mortality rates globally. The World Health Organization estimates that 11 million burns and scalds of various types occur every year and that 180 000 people die

every year from these injuries worldwide.¹⁰ Infection remains the most common complication and the most common cause of death in patients with burns of all ages, accounting for 60% to 75% of burn-related mortality.^{11,12} In response to this issue, scientists worldwide have begun developing antibacterial wound dressings that can prevent wound infection. In addition to traditional antibiotics, other types of antimicrobial agents, such as quaternary ammonium compounds, metal ions, nanoparticles, and antimicrobial polymers, have been added to wound dressings in several studies and products.^{13–15} However, antibiotics remain the mainstay of clinical treatment for wound infection, despite bacterial resistance to antibiotics becoming a growing public health issue. Of the various antibiotics used in wound dressings, tetracycline, ciprofloxacin, gentamicin, and sulfadiazine have been the most frequently

Received: December 7, 2022

Accepted: March 3, 2023

Published: March 10, 2023



employed.¹⁶ A triple-antibiotic ointment containing neomycin, polymyxin B, and bacitracin has been available as a prescription product in the United States since the 1950s and has been used as an over-the-counter product for preventing infection in superficial wounds (cuts, scrapes, and burns) since the 1970s. Studies investigating the combination of these three antibiotics have demonstrated a high degree of synergy and activity against the most common pathogens in wounds and on the skin and that resistance to the combination is unlikely.^{17,18} With the continual emergence of drug-resistant pathogens in community and hospital settings, the use of multiple synergistic antibiotics for prophylaxis or treatment is being considered.¹⁹

A wound provides a protein-rich and avascular environment that encourages the growth of pathogens while blocking host immune cells and antibiologic agents. Over a period of one week, the pathogen colony grows slowly and starts to cause infection, eventually forming a biofilm. The biofilm is usually attached to the surface of tissue or the wound. It is highly resistant to antibiotics and the host's natural immune cells. Because wound infection is a long-term process and because early symptoms of the infection are difficult to detect, a dressing that can monitor wounds for infection in real time during wound treatment would be useful for medical staff providing wound care. Ultrasound imaging is a noninvasive imaging modality that provides real-time information on tissues. High-frequency ultrasound (HFUS) is advantageous for the high-resolution imaging of tissues within a limited penetration depth; for example, it is advantageous for imaging skin and eye tissues and for imaging small animals.^{20–25} Both single-element and array transducers have been used for two-dimensional B-mode imaging and Doppler imaging.²⁶ Over the past few years, scientists have begun using sonography to predict the infection of surgical wounds. One study enrolled 49 patients, 19 of whom had peri-incisional fluid accumulation discovered through sonography. The surgical site became infected in 8 of these 19 patients, and this infection was found to be significantly associated with the ultrasound-detected collection of fluid over the wound.²⁷

The direct application of HFUS to wound infection surveillance is currently marred by several limitations. For example, when performing an ultrasound examination, the operator must apply a gel to the scanning region and then apply the ultrasound transducer to the gel. The high water content of the gel helps to guide the sound waves; this is because when ultrasonic waves arrive at the boundary between two media, a greater difference in acoustic impedance between the media results in a higher reflection coefficient. Nevertheless, applying such a gel directly to an open wound or burn may increase the risk of infection. If ultrasound scanning is performed through a wound dressing, the high ultrasound attenuation coefficients of currently used wound dressing products would result in poor imaging quality. Accordingly, to address these limitations, the present study developed a multifunctional wound dressing that not only can carry three types of antibiotics simultaneously but also has a low attenuation coefficient, rendering it suitable for ultrasound imaging. This dressing can be employed to prevent wound infection in patients with burns or large wounds and to facilitate the use of ultrasound by medical staff wishing to detect bacterial colonies without opening the dressing. This multifunctional wound dressing is expected to make a valuable

contribution to the prevention of infection in wounds and burns in the future.

2. RESULTS AND DISCUSSION

2.1. Hydrogel Loading Capacities of Three Types of Antibiotics. We determined the hydrogel loading capacities of three types of antibiotics through NanoDrop and high-performance liquid chromatography. We used NanoDrop and high-performance liquid chromatography (HPLC) to determine the neomycin sulfate, bacitracin, and polymyxin B content of the developed antibiotic hydrogel. The supernatant remaining after hydrogel cross-linking was employed to test the drugs' encapsulation. After 2 h of cross-linking, we calculated the efficiency of neomycin sulfate encapsulation in the hydrogel, which was approximately 94%. HPLC revealed that the encapsulation efficiency for bacitracin was approximately 97%, whereas that for polymyxin B was approximately 88% (Table 1). Each 10 cm × 10 cm piece of hydrogel contained 46.84 ± 0.18 mg of neomycin sulfate, 52.54 ± 0.26 mg of bacitracin, and 5.29 ± 0.61 mg of polymyxin B (Table 1).

Table 1. Drug Encapsulation Efficiency and the Amount of Antibiotics in the Hydrogel

sample	drug loading capacity (mg)	drug encapsulation efficiency (%)
neomycin sulfate	46.84 ± 0.18	93.68 ± 0.36
bacitracin	52.54 ± 0.26	97.3 ± 0.48
polymyxin B	5.29 ± 0.61	88.18 ± 10.24

2.2. Surface Structure and Mechanical Properties of Hydrogels. We used scanning electron microscopy (SEM) to analyze the surface structure of a non-antibiotic-containing hydrogel with freeze-drying (NAH-F) and that of an antibiotic-containing hydrogel with freeze-drying (AH-F). The SEM results indicated that on both the surface and in the cross sections the structure of NAH-F [Figure 1(b)] was smoother and neater than that of AH-F [Figure 1(a)]. To determine the mechanical properties of the hydrogels, a tensile test was performed to obtain their elastic modulus, tensile strength, and degree of elongation upon breakage. NAH-F was found to have a maximum stress of 14.842 MPa and a strain of 20.67% [Figure 1(c)], whereas AH-F had a maximum stress of 13.321 MPa and a strain of 21.27% [Figure 1(d)]. A rehydrated non-antibiotic-containing hydrogel (rNAH) and a rehydrated antibiotic-containing hydrogel (rAH) were also tested. The results revealed that rNAH achieved a maximum stress of 3.7603 MPa and a strain of 109.92% [Figure 1(e)], whereas rAH had a maximum stress of 3.1836 MPa and a strain of 67.123% [Figure 1(f)].

2.3. Hydrogel Swelling Capacity and Drug Release Assay. We compared the hydrogel swelling capacity of rNAH and rAH. Over a period of 0.5–24 h, rNAH exhibited a superior swelling capacity compared to rAH and gradually became saturated; after 48 h, the degrees of swelling of the two hydrogels were nearly identical [Figure 2(a)].

The drug release data suggested that antibiotics loaded into rAH were released slowly for up to 48 h. Approximately 94.26% of the neomycin sulfate, 77.15% of the bacitracin, and 88.29% of the polymyxin B had been released at 48 h [Figure 2(b)].

2.4. In Vitro Cytocompatibility of rAH and Antibacterial Activity Assays. We characterized the in vitro

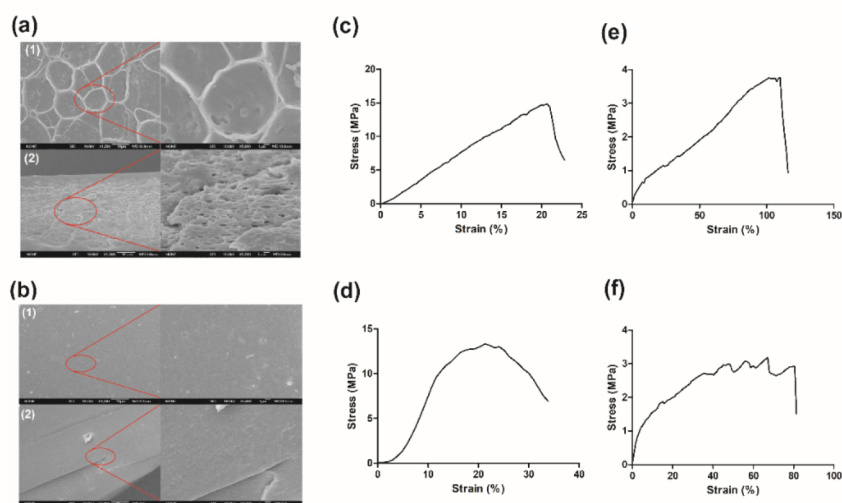


Figure 1. SEM imaging of specimens (a) AH-F and (b) NAH-F, where (1) shows the hydrogel surface imaging while (2) shows cross-sectional imaging. Tensile tests of hydrogels (c) NAH-F, (d) AH-F, (e) rNAH, and (f) rAH.

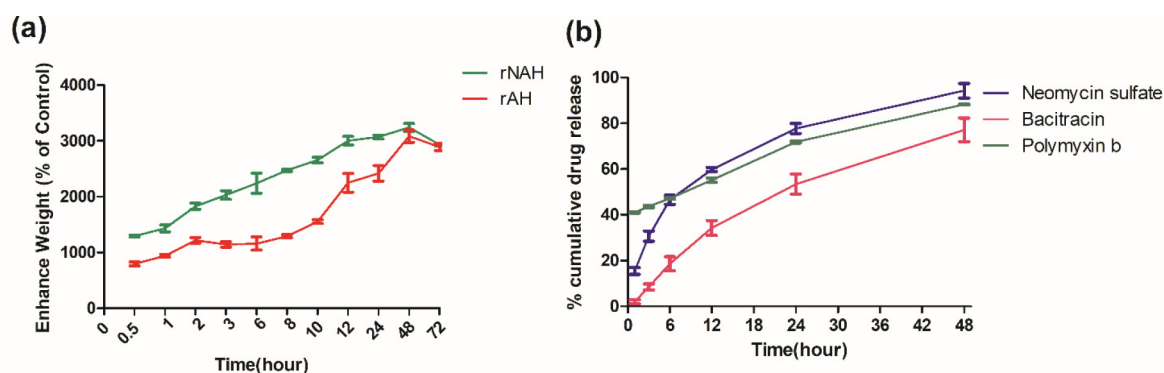


Figure 2. (a) Swelling rates for rNAH and rAH. (b) Antibiotic release rate for rAH.

cytocompatibility of the antibiotic hydrogels using the NIH-3T3 cell line and CCK-8 assay, and we determined their toxicity by measuring living cells' absorbance of 450 nm light. As displayed in Figure 3(a), the cell viability was higher than 80% between 6 and 72 h. To confirm the antibacterial ability of rAH, the corresponding inhibition zone against a bacterium was calculated. The results revealed that the inhibition zone against *Escherichia coli* was 20.43 ± 0.4 mm, and the inhibition zone against *Pseudomonas aeruginosa* was 20.52 ± 0.08 mm. Therefore, rAH had major antibacterial effects against both *E. coli* and *P. aeruginosa*, but rNAH had no antibacterial effect [Figure 3(b and c)]. After the excised agar was treated and cultured, rNAH had no antibacterial effect on either *E. coli* or *P. aeruginosa*, while rAH had significant antibacterial properties [Figure 3(d)].

2.5. Attenuation Coefficients and Imaging Quality of Hydrogels and Commercial Synthetic Dressings. We compared the signal attenuation of conventional artificial skin (Comfeel plus dressing; Coloplast), a Suprasorb H wound dressing (L&R), a Tegaderm hydrocolloid thin dressing (3M), rAH, and rNAH at various ultrasound frequencies. As illustrated in Figure 4(a), the attenuation of ultrasound signals in the HFUS B-mode was much lower for both rAH and rNAH than for the commercially available artificial dressings. Regardless of the type of material, we noted little change in the ultrasound frequency decay beyond 40 MHz [Figure 4(a)].

A higher ultrasound frequency indicates a lower penetration ability but a higher analytical value. Accordingly, 30 MHz was selected as the main measurement frequency for the subsequent experiments. The attenuation coefficient of rAH was discovered to be 0.054 dB/(mm·MHz), and that of rNAH was 0.06 dB/(mm·MHz). By contrast, the attenuation coefficients of the three commercially available artificial dressings were 0.27, 1.59, and 0.48 dB/(mm·MHz) (Table 2). Figure 4(b) depicts HFUS B-mode images, revealing that the commercial dressings lost their HFUS B-mode imaging capability at 30 MHz. To evaluate the quality of HFUS images, we calculated the corresponding signal-to-noise ratio (SNR) and contrast-to-noise ratio (CNR) values for water (normal medium), rAH, rNAH, and the three commercially available artificial dressings. The SNR and CNR values for water were both 32.09 ± 0.17 dB. Moreover, the SNR and CNR values for rAH were 18.39 ± 0.27 and 18.27 ± 0.27 dB, respectively, and those for rNAH were 18.64 ± 0.26 and 18.52 ± 0.27 dB, respectively (Table 3). By contrast, the SNR and CNR values for the Comfeel plus dressing were 5.19 ± 0.07 and 1.47 ± 0.17 dB, respectively; those for the Suprasorb H wound dressing were 5.15 ± 0.02 and 1.37 ± 0.04 dB, respectively; and those for the Tegaderm hydrocolloid thin dressing were 5.16 ± 0.11 and 1.42 ± 0.26 dB, respectively.

2.6. HFUS B-Mode Scans of Human Skin through a Hydrogel and Artificial Skin. We performed HFUS B-mode

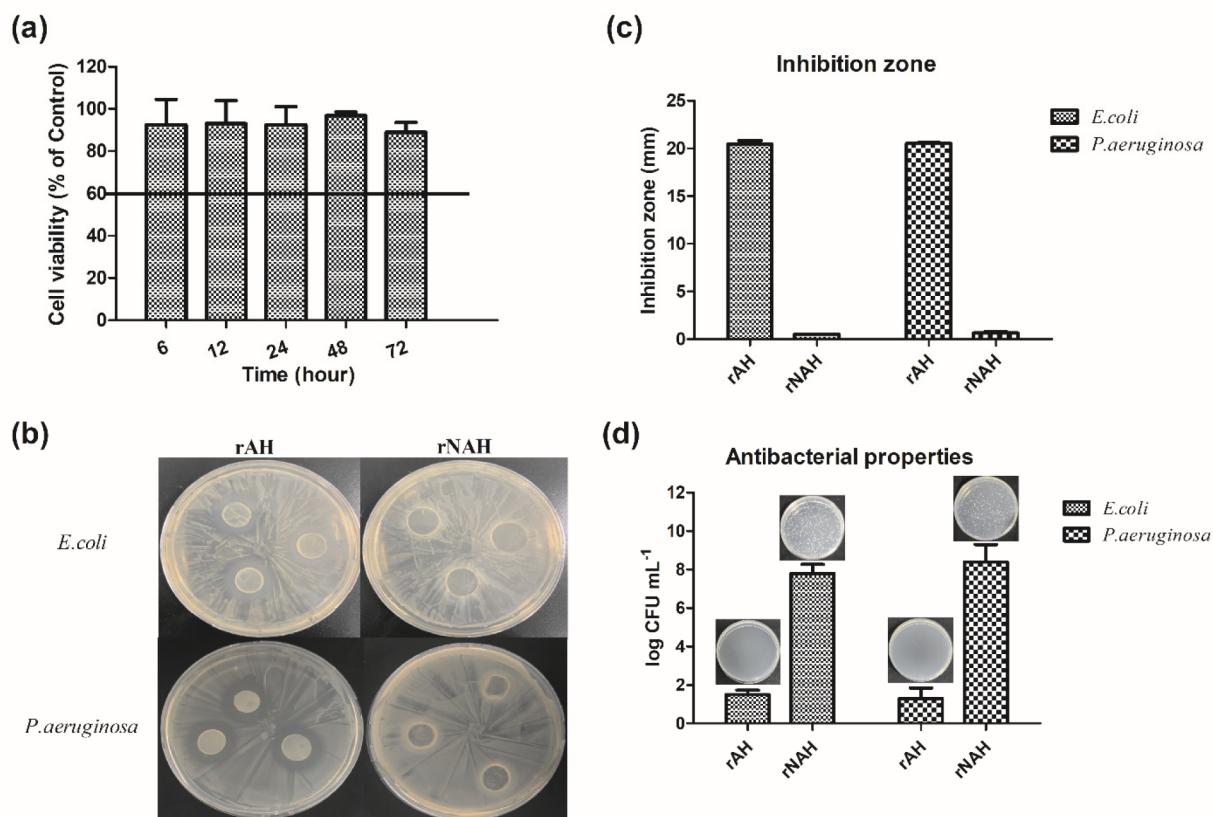


Figure 3. (a) Cytocompatibility of rAH. (b) Inhibition zone of *E. coli* and *P. aeruginosa*. (c) Mean diameter of the inhibition zone calculated from (b). (d) Antibacterial properties of rAH and rNAH.

imaging to scan the skin of a human arm through different ultrasonic media and thus test the corresponding imaging quality. Considering the ultrasonic hydrogel as the control group [Figure 5(a)(1)], we discovered that HFUS B-mode imaging was not possible through any of the investigated types of artificial skin [Figure 5(a)(2–4)]. By contrast, when the self-developed hydrogel was used, we could clearly distinguish each layer of human skin [Figure 5(b)(1–4)].

2.7. Detection of Bacterial Colonies through rAH Using HFUS B-Mode Imaging. Considering the data obtained from the scans conducted through the human skin, we employed HFUS B-mode imaging, conducted through rAH, to observe the growth of various bacterial colonies. We cultured *E. coli* and *P. aeruginosa* at a concentration of 10^8 on agar [Figure 6(a)]. The sub-area surrounded by the red circle in Figure 6 is the colony. The position and size of the colony could be easily observed in the derived HFUS B-mode image. To realistically simulate the detection of colonies in skin tissue using HFUS B-mode imaging conducted through rAH [Figure 6(b)], we purchased pork from a local market to simulate human skin tissue, inserted colonies into the pork dermis, and then covered the pork with rAH and commercially available dressings; we subsequently assessed whether HFUS B-mode imaging could detect the colonies through the dressings. The HFUS B-mode images of pork covered by rAH clearly depicted the dermal structure and inserted colonies. By contrast, the images of pork covered by the commercially available dressings depicted only a reflection of the dressings' contour; the dermal structure of the pork and the inserted colonies were not visible.

3. DISCUSSION

Wound infection remains the most common complication and cause of death in patients with burns.^{11,12} The resistance of bacteria to antibiotics has become a growing public health problem worldwide. Despite the availability of dressings that carry other types of antimicrobial agents, such as quaternary ammonium compounds, metal ions, nanoparticles, and antimicrobial polymers, as well as the commercial availability of some relevant products,^{13–15} antibiotics remain the mainstay of clinical treatment for wound infection. Owing to the increasing overuse of antibiotics, various synergistic antibiotics have been used in clinical settings to prevent or treat wound infection.¹⁹ In this study, we prepared a hydrogel containing three antibiotics simultaneously and determined that each 10 cm × 10 cm piece of our hydrogel contained 46.84 ± 0.18 mg of neomycin sulfate, 52.54 ± 0.26 mg of bacitracin, and 5.29 ± 0.61 mg of polymyxin B (Table 1). To determine whether such doses are sufficient for clinical use, we used Spersin ointment as a reference model. This ointment is used clinically to prevent and relieve skin infection caused by cuts, scrapes, and burns. Each gram of Spersin ointment contains 3.5 mg of neomycin sulfate, 400 units of bacitracin, and 5000 units of polymyxin B. According to the international standards for bacitracin²⁸ and polymyxin B,²⁹ the international unit of bacitracin is defined as 1 U = 0.01351 mg and that of polymyxin B is defined as 1 U = 0.000127 mg, respectively. Therefore, through conversion, one can determine that 10 g of Spersin ointment contains 35 mg of neomycin sulfate, 54.04 mg of bacitracin, and 6.35 mg of polymyxin B. The doses carried by our hydrogel are thus similar to those in Spersin

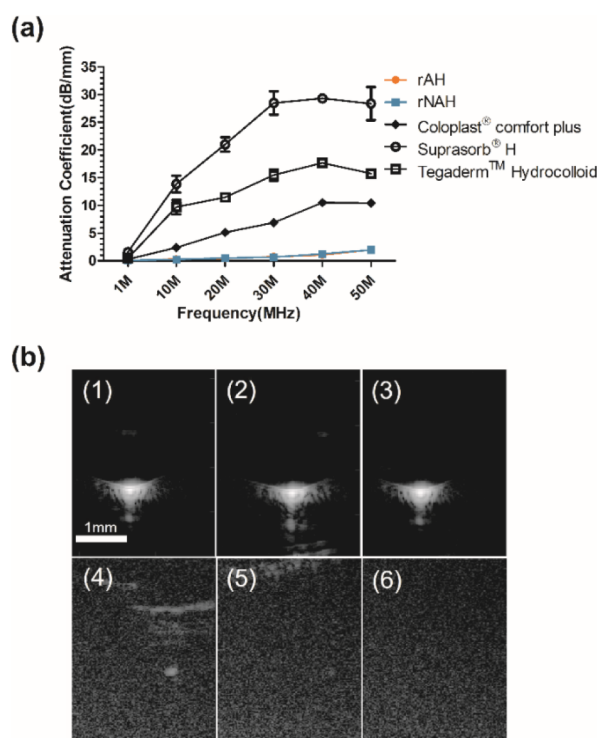


Figure 4. (a) Attenuation coefficients of hydrogels and artificial skin at various frequencies in HFUS B-mode. (b) HFUS B-mode imaging of a wire phantom was performed at 30 MHz through hydrogels and artificial skins as follows: (1) normal, (2) rAH, (3) rNAH, (4) Coloplast comfort plus, (5) Suprasorb H, and (6) Tegaderm hydrocolloid.

Table 2. Attenuation Coefficients and Thickness of Hydrogels and Artificial Skin

materials	attenuation coefficient (dB/mm/MHz)	thickness (mm)
rAH	0.054 ± 0.0071	0.6
rNAH	0.060 ± 0.023	0.6
Coloplast comfort plus	0.27 ± 0.0232	0.3
Suprasorb H	1.591 ± 0.1898	0.77
Tegaderm hydrocolloid	0.488 ± 0.0515	0.45

Table 3. SNR and CNR Values for the Hydrogels and Artificial Skin

materials	SNR (dB)	CNR (dB)
normal	32.09 ± 0.17	32.09 ± 0.17
rAH	18.39 ± 0.27	18.27 ± 0.27
rNAH	18.64 ± 0.26	18.52 ± 0.27
Coloplast comfort plus	5.19 ± 0.07	1.47 ± 0.17
Suprasorb H	5.15 ± 0.02	1.37 ± 0.04
Tegaderm Hydrocolloid	5.16 ± 0.11	1.42 ± 0.26

ointment and should be sufficient to prevent bacterial infection of wounds. We performed the disk diffusion antibiotic sensitivity test to examine the susceptibility of two bacteria, *E. coli* and *P. aeruginosa*, to the three antibiotics released by rAH. By calculating the size of the inhibition zone, we could determine whether the organism was susceptible or resistant to the antibiotics. Our results indicate that the rAH inhibition zone against both *E. coli* and *P. aeruginosa* could reach >20 mm [Figure 3(b and c)]. By comparison, when only neomycin was

carried by rAH, the inhibition zone against *E. coli* was approximately 16.33 ± 0.6 mm. According to the “Antimicrobial Disk Diffusion Zone Interpretation Guide”, the antibacterial effect of a combination of multiple antibiotics is significantly stronger than that of a single antibiotic.³⁰ We then serially diluted and incubated the treated agar to observe further antibacterial properties. It can be seen that the antibacterial properties of rAH and rNAH have extremely significant differences, regardless of whether *E. coli* or *P. aeruginosa* is used [Figure 3(d)].

We observed that NAH-F had a smoother and neater structure than AH-F, both on the surface and in the cross sections. In addition, we noted the presence of irregularly distributed pores in AH-F, which may have been caused by the presence of antibiotics during the ionic cross-linking of Ca^{2+} with alginate to form the hydrogel. The rAH hydrogel had higher porosity than rNAH, which can result in stronger absorption of tissue fluid. Our mechanical test results reveal that after freeze-drying, both the hydrogel with antibiotic loading [Figure 1(e)] and that without antibiotic loading [Figure 1(f)] were harder and less resistant to stretching than the rehydrated hydrogels. We found that the hydrogel was softer and more ductile after rehydration; this feature thus renders the hydrogel useful for application as a dressing.

The swelling rate is a critical technical feature of hydrogels. Our swelling test results indicate that rNAH and rAH had different swelling rates [Figure 2(a)]; the swelling rate of rNAH increased steadily and reached saturation at 48 h. By contrast, rAH had a lower adsorption rate at the beginning, but the swelling rate increased after 10 h and reached saturation at 48 h. On the basis of a comparison of the drug release data [Figure 2(b)], we can reasonably assume that the difference in the adsorption rate was due to the rAH hydrogel still adsorbing liquid after its slow release of the antibiotics. The drug release data show that the three antibiotics in rAH were released at different rates and were released continuously for 48 h.

We performed an in vitro cytotoxicity test in accordance with ISO 10993-5. We removed rAH after 24 h of its immersion in a serum-containing culture medium, and we cultured cells in this extract to assess the hydrogel’s potential for cytotoxicity. Cell viability was estimated to be higher than 80% during the period of 6–72 h [Figure 3(a)], and the cytotoxicity level was discovered to be less than 2, which means that the hydrogel has excellent biocompatibility. Although one study reported that antibiotics can damage mammalian cells at certain concentrations,³¹ we observed that the antibiotics released by rAH did not appear to cause much damage to the cells. The hydrocolloid may have a slow-release function such that the concentration of antibiotics in the extract was not sufficiently high to induce damage to NIH3T3 cells; accordingly, the hydrocolloid itself may have excellent biocompatibility.

In clinical settings, staff cannot determine the degree of wound healing without changing the conventional wound dressing. Nevertheless, in recent years, imaging modalities such as magnetic resonance imaging, computed tomography, and ultrasound have been used clinically to detect soft tissue infection and assess wound healing.³² The advantages of ultrasound imaging over other imaging methods are that it does not expose the patient to radiation and is portable, cost-effective, and easy to use.³³ In this study, we measured the ultrasound signal attenuation coefficient of rAH, rNAH, and commercially available dressings [Figure 4(a)]. According to

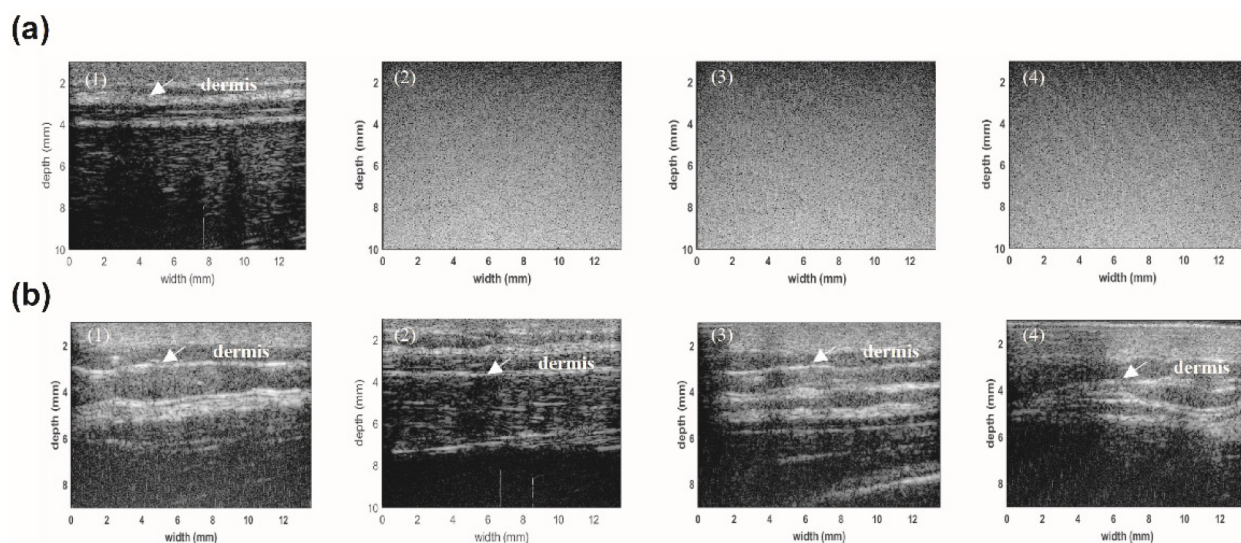


Figure 5. HFUS B-mode images of (a) human arm skin through (1) ultrasound gel, (2) Coloplast comfort plus, (3) Suprasorb H, and (4) Tegaderm hydrocolloid and (b) human arm skin through (1) rAH, (2) rNAH, (3) AH-F, and (4) NAH-F. White arrows point to dermis skin in the area.

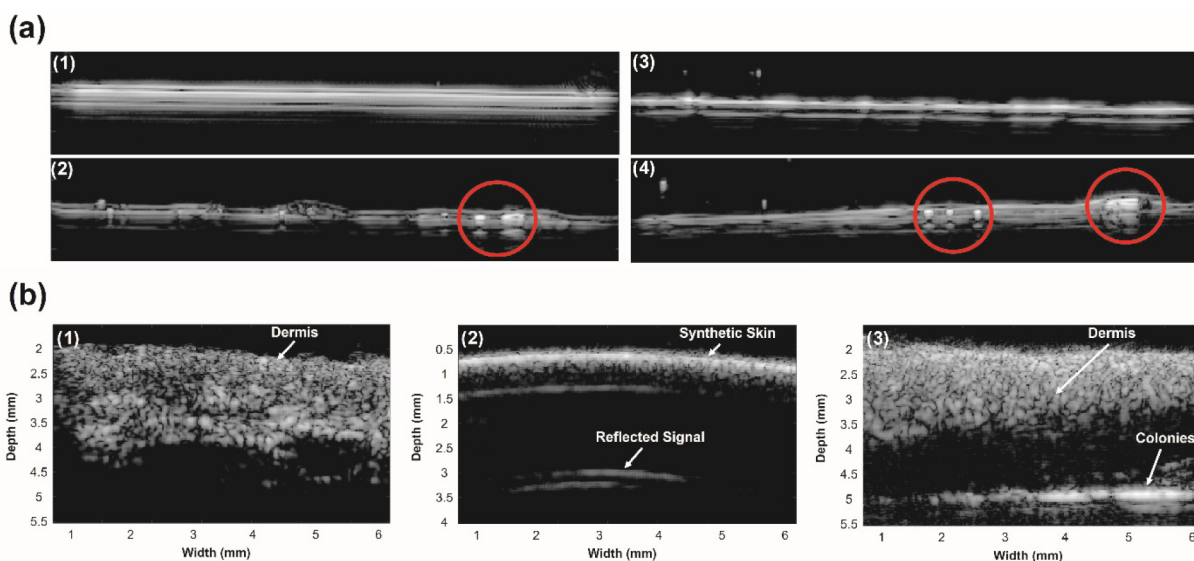


Figure 6. (a) HFUS B-mode images of rAH-covered (1) agar, (2) *E. coli* colonies on agar, (3) blood agar, and (4) *P. aeruginosa* colonies on blood agar. Colonies are indicated by red circles. (b) HFUS B-mode images of (1) pork covered with rAH and with no *E. coli* colonies on its surface, (2) pork covered with Tegaderm hydrocolloid and with *E. coli* colonies on its surface, and (3) pork covered with rAH and with *E. coli* colonies on its surface.

the experimental results, dressing thickness and ultrasonic attenuation coefficients are not directly related but depend on the material. We observed that the ultrasound attenuation coefficients of rAH and rNAH were considerably smaller than those of the commercially available dressings at small thicknesses (Table 2). To evaluate ultrasound image quality, we compared the three commercially available artificial dressings with our hydrogels at an ultrasound frequency of 30 MHz [Figure 4(b); Table 3]. We found that the hydrogels exhibited superior SNRs and CNRs compared to the other materials. In general, stronger ultrasound signals afford more accurate real-time wound condition detection.³⁴ Accordingly, to assess image quality, we employed HFUS B-mode imaging to observe human skin structures through the commercially available artificial dressings and our hydrogels. As depicted in

Figure 5, the qualities of all four images—those captured through rAH, rNAH, AH-F, and NAH-F [Figure 5(b)(1–4)]—were similar to that of the image captured using ultrasound gel alone [Figure 5(a)(1)], and the dermis structure could be clearly distinguished. By contrast, no HFUS B-mode images could be obtained through the commercially available artificial dressings under the same conditions [Figure 5(a)(2–4)].

A chronic wound provides an ideal environment for biofilm formation because necrotic tissue and debris attract bacteria, which reversibly attach to solid surfaces and quickly multiply, forming microcolonies; unlike planktonic bacteria, biofilm bacteria exhibit distinct phenotypes and are highly resistant to antibiotics.^{35,36} Consequently, identifying colony formation early in the process of wound healing can facilitate the

decision-making process and benefit early prevention efforts. In this study, we cultured *E. coli* and *P. aeruginosa* to simulate the process of colony formation. Bacterial colonies in rAH-covered agar were then imaged through HFUS B-mode imaging; the corresponding colony clusters and formation densities could be successfully observed [Figure 6(a)(2 and 4)]. Furthermore, to confirm whether in vivo colony signals could be detected through rAH in HFUS B-mode imaging, we performed cortical simulations using fresh pig skin.^{37,38} The data confirm that in both the control group and the experimental group in which rAH covered the pig skin surface, the dermal structures could be clearly observed [Figure 6(b)(1), white arrows], as could the colonies inside the transdermal layer [Figure 6(b)(3), white arrows]. However, when the commercially available artificial dressings was placed over the pig skin surface, HFUS B-mode images did not show the dermis structures or the inserted colonies [Figure 6(b)(2)]. As depicted in Figure 6(b)(2), only strong reflected signals were observed, which is probably due to the strong attenuation characteristic of the artificial skin.³⁹

4. CONCLUSIONS

In this study, we successfully prepared a hydrogel containing three antibiotics simultaneously and demonstrated that it exhibited favorable antibacterial properties. Not only can it replace the antibacterial effect of the ointment currently on the market but it can also be modified into a hydrogel dressing, which is easier to use than the ointment type. Coloplast, Suprasorb, and Tegaderm are all wound dressings, the main purpose which is to protect the wound; if it is necessary to prevent wound infection, they still need to be used in combination with drugs. The hydrogel we developed not only has the effect of preventing wound infection but also improves it into a dressing mode. In short, it is a material that can replace the dressings and ointments currently used clinically. Furthermore, we determined that this hydrogel had a lower attenuation coefficient than conventional artificial skin, meaning that HFUS B-mode imaging could be performed through the hydrogel to instantly detect infection in a wound. Currently, clinicians can only judge recovery from the appearance of the wound and cannot immediately know whether the wound is infected. Therefore, we focused on detecting early bacterial infections using ultrasound. Ultrasound can detect subcutaneous colony formation, helping clinicians plan treatment as quickly as possible. The proposed hydrogel is thus highly advantageous for wound dressing applications—not only for chronic wounds, but also for wounds that have become infected due to an implant.

5. METHODS

5.1. Fabrication of a Hydrogel Loaded with Multiple Antibiotics. A sodium alginate hydrogel was prepared using 0.2 g of sodium alginate (Sigma-Aldrich, USA) dissolved in 10 mL of Milli-Q water to obtain the desired final concentration of 2 wt %. Subsequently, prepared mixtures of 4 mM 1-ethyl-3-(3-(dimethylamino)propyl)carbodiimide (EDC; Sigma-Aldrich, USA) were stirred at 30 °C for 2 h. The hydrogel was loaded with 50 mg of neomycin sulfate (Sigma-Aldrich, USA), 54 mg of bacitracin (Sigma-Aldrich, USA), and 6 mg of polymyxin B sulfate (Sigma-Aldrich, USA). The antibiotic pH was controlled at 8.7. Subsequently, 10 mL of 2% sodium alginate was dripped onto a dish with a 10 cm diameter and

mixed with 10 mL of the antibiotic solution, after which the dish was placed on a hot plate at 60 °C for 4 h. We used 2% calcium chloride (Sigma-Aldrich, USA) as the cross-linking agent with the sodium alginate loaded with the antibiotics, and cross-linking was performed for 2 h. The resulting mixture was stored at −80 °C in a freezer. The hydrogel was then freeze-dried for 24 h to enable it to produce additional pores.

5.2. Determination of the Antibiotic Content of the Hydrogels. NanoDrop and HPLC can be used to determine the concentration of neomycin sulfate in a preparation or product. Neomycin has no ultraviolet-absorbing chromophores, and in most methods pre- or postcolumn derivatization is conducted. However, derivatization procedures are difficult to perform and cause problems during quantification.⁴⁰ Therefore, we attempted to determine the optimal conditions under which to release the adsorbed neomycin and quantify it through spectrophotometry after the 2,4-dinitrofluorobenzene (DNFB; Sigma-Aldrich, USA) reaction. The reaction between the neomycin solution and DNFB was performed in triplicate. From each original solution and the blanks, a 1 mL aliquot (the supernatant) was transferred to a 1 mL Eppendorf tube. Color was developed by adding 0.4 mL of 0.25% methanolic solution of DNFB. After 50 min under ambient conditions, 0.3 mL of 1.0 M HCL was added to each tube, and the absorbance was measured at 360 nm.⁴¹ In the HPLC determination of bacitracin, the stationary phase was a Zorbax eclipse C18 column (250 mm × 4.6 mm and with average particle size of 5 μm). The mobile phase consisted of 5 mM ammonium acetate buffer (solvent A; pH 5.5) and 100% acetonitrile (solvent B). The gradient elution was performed as follows: 5% to 45% solvent B over 40 min, 45% to 90% solvent B over 12 min, and 90% to 5% solvent B over 8 min, with the flow rate maintained at 1.0 mL/min. The samples were injected, and the peaks at 220 nm were analyzed.⁴² In the HPLC determination of polymyxin b, the stationary phase was a Zorbax Eclipse plus C18 column (4.6 mm × 250 mm), with a mobile phase consisting of 0.1 M Na₂HPO₄ (adjusted to pH 3.0 with HCL) and acetonitrile (in a ratio of 77:23) at a flow rate of 1.0 mL/min for 25 min; the eluent's absorbance at 212 nm was monitored.⁴³

Equation 1 shows the formula for calculating the encapsulation efficacy (E.E.; %).

$$\text{E.E. (\%)} = \frac{\text{Drug content of hydrogel (mg)}}{\text{Initial amount of drug (mg)}} \times 100\% \quad (1)$$

5.3. In Vitro Drug Release Study. An in vitro drug release study was performed on the basis of the method detailed in previous studies, with a slight modification.^{44–46} In brief, AH-F was sealed on a Cellu-Sep T4 dialysis bag (Mw: 12 000–14 000; Membrane Filtration Products, Inc., USA) and incubated in 20 mL of 1× phosphate-buffered saline (PBS) (pH 7.4) in a 37 °C water bath. At 1, 3, 6, 12, 24, and 48 h, samples of volume 3 mL were withdrawn from the released solution, and their drug concentrations were analyzed to determine the drug encapsulation efficiency. After each sampling, 3 mL of fresh PBS was added to the solution. All samples were obtained in triplicate, and average values were calculated. The drug release efficiency percentage (R.E.) is expressed as the percentage of the drug released by AH-F in relation to the amount of drug the hydrogel contained.

Equation 2 shows the formula for calculating the drug release efficiency (R.E.; %).

$$\text{R.E. (\%)} = \frac{\text{Drug releasing from AH-F (mg)}}{\text{Drug content of AH-F (mg)}} \times 100\% \quad (2)$$

5.4. Morphological Analysis. The samples were analyzed using a high-resolution field-emission scanning electron microscope (SU8010; Hitachi, Japan) operated under high vacuum at 0.5–30 kV. Images were obtained by observing the surface configuration in low-voltage electron imaging and secondary electron imaging. Each sample was immersed in liquid nitrogen and fractured, enabling its surface and cross-sectional shape to be observed. All samples were spun and coated with a thin layer of gold prior to the analysis.⁴⁷

5.5. Tensile Testing of the Hydrogels. The mechanical properties of the hydrogels were analyzed through a tensile test. Four samples of each composition of hydrogel were cut into the shape of a dog bone in accordance with the ASTM D638-99 standard. A universal testing machine was used to perform each test with a 10 N loading cell. Samples were tested at a crosshead rate of 2 mm/min until failure. The fracture strength (σ_F) and secant modulus values at low strain (E) were calculated.

Equation 3 shows the formula for calculating the Young's modulus, where E is Young's modulus, σ is the stress, and ε is strain.

$$E = \frac{\sigma}{\varepsilon} \quad (3)$$

5.6. Water Absorption Efficacy Measurements. Each hydrogel was cut into a square sample (1 cm × 1 cm). The sample was then placed on a dry disc at room temperature. The sample was weighed and placed in 1 mL of PBS at neutral pH (pH = 7.4), after which it was placed in an incubator at 37 °C for various durations. The sample was gently removed from the buffer solution, excess buffer solution on the sample surface was dried using filter paper, and the sample was weighed.

Equation 4 shows the formula for calculating water absorption, where W_s and W_d are the weights of the swollen and dry samples, respectively.⁴⁸

$$\text{Water Absorption} = \frac{W_s - W_d}{W_d} \times 100\% \quad (4)$$

5.7. Antimicrobial Analysis. The activity of the hydrogels against *E. coli* (ATCC 13706) and *P. aeruginosa* (ATCC 27853) was investigated. In the agar disc diffusion method, 100 μL of the suspension of each bacterium was evenly smeared at a concentration of 10^8 CFU/mL onto a hydrogel disc of diameter 10 mm that was placed on an agar disc. These bacterium samples were incubated for 24 h at 37 °C, and the inhibition zone around each sample was calculated using ImageJ software. This zone was used as a criterion indicating the antibacterial properties of the components.⁴⁹ Remove the agar, which is the same size as the hydrogel, and place it in 5 mL of PBS to dissolve the colony in it. Next, perform the step of serial dilution, and then take 100 μL each to the LB agar for coating. After overnight incubation, count the number of colonies and calculate the initial concentration.

5.8. Cell Cytotoxicity Assay. The viability of cells in contact with antibiotic-containing hydrogels was tested using the CCK-8 assay (TargetMol, USA) on NIH-3T3 cells. Before the analysis, the hydrogel samples were sterilized under ultraviolet radiation and soaked in the culture medium. Cells (5×10^3 cells/cm²) were seeded on 96-well plates containing

each sample and incubated in a humidity chamber (5% CO₂, 37 °C, and 95% humidity) for 24 h. The number of viable cells in the population was measured at the time points of 1, 3, 6, 12, 24, 48, and 72 h after the addition of the mixture medium. Before testing was performed, 90 μL of the original medium was removed, and 10 μL of CCK-8 was added to each well before the measurement at each test time; this was followed by storage in a humidity chamber for 2 h.⁵⁰ Finally, absorbance density measurements were conducted using an enzyme-linked immunosorbent assay reader (DeTie, China) at a wavelength of 450 nm, and cell viability was calculated as follows:

Equation 5 shows the formula for calculating cell viability

$$\text{Cell viability} = \frac{\text{OD}_{\text{tested}}}{\text{OD}_{\text{control}}} \times 100\% \quad (5)$$

5.9. Ultrasound Attenuation Coefficient. The attenuation coefficients of the materials were measured using the substitution method.^{51,52} The attenuation coefficients of the hydrogels and artificial dressings at a particular frequency were measured by calculating amplitude changes from the lower parallel disc. In the formula, d represents the thickness of the material and $A_1(f)$ and $A_2(f)$ represent the amplitudes of the echo spectrum of the lower disc in distilled water with and without samples, respectively. The spectrum was determined using the fast Fourier transform algorithm.

Equation 6 shows the formula for calculating the attenuation coefficient (α).

$$\alpha = \frac{20 \log_{10}(A_1(f)/A_2(f))}{2d} \quad (6)$$

5.10. Wire Phantom on Material. HFUS (40 MHz) imaging was performed in accordance with the method discussed in our previous article.⁵³ Each of the hydrogels or artificial dressings was placed on a wire phantom, and HFUS B-mode imaging was then conducted to determine the contrast of the derived ultrasound image. Two regions of interest (ROIs) were selected to calculate SNR and CNR, where \bar{P}_{wire} and \bar{P}_{bck} are the mean power of the wire and background clutter signals, respectively, which were derived from the ROIs, and σ_{noise} is the standard deviation of the background clutter signals.

Equation 7 shows the formula for calculating the SNR.⁵⁴

$$\text{SNR} = 10 \cdot \log_{10} \left(\frac{\bar{P}_{\text{wire}}}{\sigma_{\text{noise}}} \right) \quad (7)$$

Equation 8 shows the formula for calculating the CNR.⁵⁵

$$\text{CNR} = 10 \cdot \log_{10} \left(\frac{|\bar{P}_{\text{wire}} - \bar{P}_{\text{bck}}|}{\sigma_{\text{noise}}} \right) \quad (8)$$

5.11. HFUS B-Mode Imaging of Human Skin. We compared ultrasound gel, rAH, rNAH, AH-F, and NAH-F by performing HFUS imaging. We placed each material on the arm of volunteer and then conducted HFUS B-mode imaging.

5.12. Detection of Bacterial Colonies in HFUS B-Mode Images. *E. coli* and *P. aeruginosa* were dispersed at a concentration of 10^4 CFU/mL on agar discs and blood agar discs. The colonies were then covered by hydrogel after 1 day of culturing, and HFUS imaging was performed. By continually acquiring B-mode images, we used this system to track every colony. In the simulation involving pig skin, cultured colonies were transplanted onto pig skin using a loop, and the

uppermost layer of the skin was then covered with hydrogel or artificial skin; subsequently, B-mode images were continually acquired.

AUTHOR INFORMATION

Corresponding Author

Ping-Ching Wu – Department of Biomedical Engineering, Medical Device Innovation Center, Center of Applied Nanomedicine, and Institute of Oral Medicine and Department of Stomatology, National Cheng Kung University Hospital, College of Medicine, National Cheng Kung University, Tainan 701401, Taiwan; Email: wbcxyz@bme.ncku.edu.tw

Authors

Yao-Wei Yeh – Department of Biomedical Engineering, National Cheng Kung University, Tainan 701401, Taiwan; orcid.org/0000-0001-8349-3637

Chih-Chung Huang – Department of Biomedical Engineering and Medical Device Innovation Center, National Cheng Kung University, Tainan 701401, Taiwan

Wen-Shuo Kuo – Center for Allergy, Immunology and Microbiome (AIM), China Medical University Children's Hospital/China Medical University Hospital, China Medical University, Taichung 404327, Taiwan

Tzu-Lung Liao – Department of Biomedical Engineering, National Cheng Kung University, Tainan 701401, Taiwan

Tsung-Lin Tsai – Department of Biomedical Engineering, Department of Oncology, National Cheng Kung University Hospital, College of Medicine, and Center of Applied Nanomedicine, National Cheng Kung University, Tainan 701401, Taiwan

Complete contact information is available at: <https://pubs.acs.org/10.1021/acsomega.2c07806>

Author Contributions

Y.W.Y., C.C.H., W.S.K., T.L.T., and P.C.W. designed the study; Y.W.Y. and L.T.L. performed the experiments; Y.W.Y. and L.T.L. contributed to the characterization and data analysis; and Y.W.Y., C.C.H., and P.C.W. wrote the paper. All the authors provided comments on the paper.

Notes

The authors declare no competing financial interest.

ACKNOWLEDGMENTS

Funding was supported by the National Science and Technology Council (NSTC) under project numbers 110-2221-E-006-013-MY3, 110-2314-B-039-056-MY3 and 111-2113-M-039-003-MY2; the Center of Applied Nanomedicine and the Medical Device Innovation Center of National Cheng Kung University; the Special Field Research Center Program within the framework of the Taiwan Ministry of Education's Higher Education Emerging Project; and the Center for Allergy Immunology and Microbiome (A.I.M.), China Medical University Hospital/China Medical University Children's Hospital, China Medical University, Taiwan (1JA8; DMR-112-141). The authors thank the i-MANI Center, National Biopharmaceutical Core Facility, NSTC, Taiwan, and the Instrument Development Center for technical assistance.

REFERENCES

- (1) Ramos-e-Silva, M.; Ribeiro de Castro, M. C. New dressings, including tissue-engineered living skin. *Clin. Dermatol.* **2002**, *20* (6), 715–723.
- (2) Caló, E.; Khutoryanskiy, V. V. Biomedical applications of hydrogels: A review of patents and commercial products. *Eur. Polym. J.* **2015**, *65*, 252–267.
- (3) Pott, F. S.; Meier, M. J.; Stocco, J. G.; Crozeta, K.; Ribas, J. D. The effectiveness of hydrocolloid dressings versus other dressings in the healing of pressure ulcers in adults and older adults: a systematic review and meta-analysis. *Rev. Lat. Am. Enfermagem* **2014**, *22* (3), 511–520.
- (4) Bhattarai, S. R.; Bhattarai, N.; Yi, H. K.; Hwang, P. H.; Cha, D. I.; Kim, H. Y. Novel biodegradable electrospun membrane: scaffold for tissue engineering. *Biomaterials* **2004**, *25* (13), 2595–2602.
- (5) Kamoun, E. A.; Kenawy, E. S.; Chen, X. A review on polymeric hydrogel membranes for wound dressing applications: PVA-based hydrogel dressings. *J. Adv. Res.* **2017**, *8* (3), 217–233.
- (6) Hou, S.; Lake, R.; Park, S.; Edwards, S.; Jones, C.; Jeong, K. J. Injectable Macroporous Hydrogel Formed by Enzymatic Cross-Linking of Gelatin Microgels. *ACS Appl. Bio Mater.* **2018**, *1* (5), 1430–1439.
- (7) Morgan, D. Alginate Dressings: Part 1: Historical Aspects. *J. Tissue Viability* **1997**, *7* (1), 4–9.
- (8) Gilchrist, T.; Martin, A. M. Wound treatment with Sorbsan—an alginate fibre dressing. *Biomaterials* **1983**, *4* (4), 317–320.
- (9) Berridge, M. J. Calcium signalling and cell proliferation. *Bioessays* **1995**, *17* (6), 491–500.
- (10) Burns. World Health Organization, 2018. <https://www.who.int/en/news-room/fact-sheets/detail/burns> (accessed 2018-03-06).
- (11) Church, D.; Elsayed, S.; Reid, O.; Winston, B.; Lindsay, R. Burn wound infections. *Clin. Microbiol. Rev.* **2006**, *19* (2), 403–434.
- (12) Gomez, R.; Murray, C. K.; Hospenthal, D. R.; Cancio, L. C.; Renz, E. M.; Holcomb, J. B.; Wade, C. E.; Wolf, S. E. Causes of mortality by autopsy findings of combat casualties and civilian patients admitted to a burn unit. *J. Am. Coll. Surg.* **2009**, *208* (3), 348–354.
- (13) Wu, P.-C.; Chen, H.-H.; Chen, S.-Y.; Wang, W.-L.; Yang, K.-L.; Huang, C.-H.; Kao, H.-F.; Chang, J.-C.; Hsu, C.-L. L.; Wang, J.-Y.; et al. Graphene oxide conjugated with polymers: a study of culture condition to determine whether a bacterial growth stimulant or an antimicrobial agent? *J. Nanobiotechnology* **2018**, *16*, 1.
- (14) Song, D. W.; Kim, S. H.; Kim, H. H.; Lee, K. H.; Ki, C. S.; Park, Y. H. Multi-biofunction of antimicrobial peptide-immobilized silk fibroin nanofiber membrane: Implications for wound healing. *Acta Biomater.* **2016**, *39*, 146–155.
- (15) Homaeigohar, S.; Boccaccini, A. R. Antibacterial biohybrid nanofibers for wound dressings. *Acta Biomater.* **2020**, *107*, 25–49.
- (16) Simões, D.; Miguel, S. P.; Ribeiro, M. P.; Coutinho, P.; Mendonça, A. G.; Correia, I. J. Recent advances on antimicrobial wound dressing: A review. *Eur. J. Pharm. Biopharm.* **2018**, *127*, 130–141.
- (17) Jones, R. N.; Li, Q.; Kohut, B.; Biedenbach, D. J.; Bell, J.; Turnidge, J. D. Contemporary antimicrobial activity of triple antibiotic ointment: a multiphased study of recent clinical isolates in the United States and Australia. *Diagn. Microbiol. Infect. Dis.* **2006**, *54* (1), 63–71.
- (18) Booth, J. H.; Benrimoj, S. I.; Nimmo, G. R. In vitro interactions of neomycin sulfate, bacitracin, and polymyxin B sulfate. *Int. J. Dermatol.* **1994**, *33* (7), 517–520.
- (19) Bonomo, R. A.; Van Zile, P. S.; Li, Q.; Shermock, K. M.; McCormick, W. G.; Kohut, B. Topical triple-antibiotic ointment as a novel therapeutic choice in wound management and infection prevention: a practical perspective. *Expert Rev. Anti Infect. Ther.* **2007**, *5* (5), 773–782.
- (20) Shih, C. C.; Chen, P. Y.; Ma, T.; Zhou, Q.; Shung, K. K.; Huang, C. C. Development of an intravascular ultrasound elastography based on a dual-element transducer. *R Soc. Open Sci.* **2018**, *5* (4), 180138.

- (21) Liu, T.-Y.; Lee, P.-Y.; Huang, C.-C.; Sun, L.; Shung, K. K. A study of the adult zebrafish ventricular function by retrospective Doppler-gated ultrahigh-frame-rate echocardiography. *IEEE Trans Ultrason, Ferroelect., Freq. Contr.* **2013**, *60* (9), 1827–1837.
- (22) Tsai, W. Y.; Hsueh, Y. Y.; Chen, P. Y.; Hung, K. S.; Huang, C. C. High-Frequency Ultrasound Elastography for Assessing Elastic Properties of Skin and Scars. *IEEE Trans Ultrason Ferroelectr Freq Control* **2022**, *69* (6), 1871–1880.
- (23) Chen, P. Y.; Shih, C. C.; Lin, W. C.; Ma, T.; Zhou, Q.; Shung, K. K.; Huang, C. C. High-Resolution Shear Wave Imaging of the Human Cornea Using a Dual-Element Transducer. *Sensors (Basel)* **2018**, *18* (12), 4244.
- (24) Vogt, M.; Paul, B.; Scharenberg, S.; Scharenberg, R.; Ermert, H. Development of a high frequency ultrasound skin imaging system: optimization utilizing time domain reflectometry and network analysis. *IEEE Symp. Ultrason.* **2003**, *1*, 744–747.
- (25) Huang, C. C.; Su, T. H.; Shih, C. C. High-resolution tissue Doppler imaging of the zebrafish heart during its regeneration. *Zebrafish* **2015**, *12* (1), 48–57.
- (26) Shung, K. K. Ultrasonic transducers and arrays. In *Diagnostic Ultrasound: Imaging and Blood Flow Measurements*, 2nd ed.; CRC Press: Boca Raton, FL, 2015; pp 55–58.
- (27) Barrett, C. D.; Celestin, A.; Fish, E.; Glass, C. C.; Eskander, M. F.; Murillo, R.; Gospodinov, G.; Gupta, A.; Hauser, C. J. Surgical wound assessment by sonography in the prediction of surgical wound infections. *J. Trauma Acute Care Surg* **2016**, *80* (2), 229–236.
- (28) Humphrey, J. H.; Lightbown, J. W.; Mussett, M. V.; Perry, W. L. The international standard for bacitracin. *Bull. World Health Organ.* **1953**, *9* (6), 861–869.
- (29) Humphrey, J. H.; Lightbown, J. W.; Musset, M. V. The International Standard for polymyxin B. *Bull. World Health Organ.* **1959**, *20* (6), 1229–1232.
- (30) Odland, B. A.; Erwin, M. E.; Jones, R. N. Quality control guidelines for disk diffusion and broth microdilution antimicrobial susceptibility tests with seven drugs for veterinary applications. *J. Clin. Microbiol.* **2000**, *38* (1), 453–455.
- (31) Kovacik, A.; Tvrdá, E.; Jambor, T.; Fulopova, D.; Kovacicova, E.; Hleba, L.; Kołodziejczyk, E. M.; Hlebova, M.; Gren, A.; Massanyi, P. Cytotoxic effect of aminoglycoside antibiotics on the mammalian cell lines. *J. Environ. Sci. Health A* **2021**, *56* (1), 1–8.
- (32) Li, S.; Mohamedi, A. H.; Senkowsky, J.; Nair, A.; Tang, L. Imaging in Chronic Wound Diagnostics. *Adv. Wound Care (New Rochelle)* **2020**, *9* (5), 245–263.
- (33) Li, S.; Renick, P.; Senkowsky, J.; Nair, A.; Tang, L. Diagnostics for Wound Infections. *Adv. Wound Care (New Rochelle)* **2021**, *10* (6), 317–327.
- (34) Rodriguez-Molares, A.; Rindal, O. M. H.; D’Hooge, J.; Masoy, S. E.; Austeng, A.; Lediju Bell, M. A.; Torp, H. The Generalized Contrast-to-Noise Ratio: A Formal Definition for Lesion Detectability. *IEEE Trans Ultrason Ferroelectr Freq Control* **2020**, *67* (4), 745–759.
- (35) Zhao, G.; Usui, M. L.; Lippman, S. I.; James, G. A.; Stewart, P. S.; Fleckman, P.; Olerud, J. E. Biofilms and Inflammation in Chronic Wounds. *Adv. Wound Care (New Rochelle)* **2013**, *2* (7), 389–399.
- (36) Alharbi, N. S.; Khaled, J. M.; Kadaikunnan, S.; Alobaidi, A. S.; Sharafaddin, A. H.; Alyahya, S. A.; Almanaa, T. N.; Alsughayir, M. A.; Shehu, M. R. Prevalence of Escherichia coli strains resistance to antibiotics in wound infections and raw milk. *Saudi J. Biol. Sci.* **2019**, *26* (7), 1557–1562.
- (37) Seto, J. E.; Polat, B. E.; Lopez, R. F. V.; Blankschtein, D.; Langer, R. Effects of ultrasound and sodium lauryl sulfate on the transdermal delivery of hydrophilic permeants: Comparative in vitro studies with full-thickness and split-thickness pig and human skin. *J. Controlled Release* **2010**, *145* (1), 26–32.
- (38) Liao, A.-H.; Lin, K.-H.; Chuang, H.-C.; Tsai, C.-H.; Lin, Y.-C.; Wang, C.-H.; Shih, C.-P.; Liu, H.-L. Low-frequency dual-frequency ultrasound-mediated microbubble cavitation for transdermal minoxidil delivery and hair growth enhancement. *Sci. Rep.* **2020**, *10*, 4338.
- (39) Law, Y.; Knott, T.; Pick, S.; Weyers, B.; Kuhlen, T. Simulation-based Ultrasound Training Supported by Annotations, Haptics and Linked Multimodal Views. In *Eurographics Workshop on Visual Computing for Biology and Medicine*; Bühler, K., Linsen, L., John, N. W., Eds.; The Eurographics Association: Eindhoven, The Netherlands, 2015; pp 167–176. DOI: 10.2312/vcbm.2015.1220
- (40) Pendela, M.; Adams, E.; Hoogmartens, J. Development of a liquid chromatographic method for ear drops containing neomycin sulphate, polymyxin B sulphate and dexamethasone sodium phosphate. *J. Pharm. Biomed Anal* **2004**, *36* (4), 751–757.
- (41) Marques, M. R. C.; Hackmann, E. R. M.; Saito, T. Extraction and Spectrophotometric Determination of Neomycin Sulfate in Pharmaceutical Oral Suspensions. *Anal. Lett.* **1990**, *23* (6), 1005–1016.
- (42) Singh, H.; Kaur, M.; Jangra, M.; Mishra, S.; Nandanwar, H.; Pinnaka, A. K. Antimicrobial properties of the novel bacterial isolate Paenibacillus sp. SMB1 from a halo-alkaline lake in India. *Sci. Rep.* **2019**, *9*, 11561.
- (43) Shaheen, M.; Li, J.; Ross, A. C.; Vederas, J. C.; Jensen, S. E. Paenibacillus polymyxa PKB1 Produces Variants of Polymyxin B-Type Antibiotics. *Chem. Biol.* **2011**, *18* (12), 1640–1648.
- (44) Josef, E.; Zilberman, M.; Bianco-Peled, H. Composite alginate hydrogels: An innovative approach for the controlled release of hydrophobic drugs. *Acta Biomater.* **2010**, *6* (12), 4642–4649.
- (45) Xin, J.; Guo, Z.; Chen, X.; Jiang, W.; Li, J.; Li, M. Study of branched cationic β -cyclodextrin polymer/indomethacin complex and its release profile from alginate hydrogel. *Int. J. Pharm.* **2010**, *386* (1), 221–228.
- (46) Jeon, O.; Powell, C.; Solorio, L. D.; Krebs, M. D.; Alsberg, E. Affinity-based growth factor delivery using biodegradable, photocrosslinked heparin-alginate hydrogels. *J. Controlled Release* **2011**, *154* (3), 258–266.
- (47) Aston, R.; Sewell, K.; Klein, T.; Lawrie, G.; Grøndahl, L. Evaluation of the impact of freezing preparation techniques on the characterisation of alginate hydrogels by cryo-SEM. *Eur. Polym. J.* **2016**, *82*, 1–15.
- (48) Chaturvedi, A.; Bajpai, A. K.; Bajpai, J.; Singh, S. K. Evaluation of poly (vinyl alcohol) based cryogel-zinc oxide nanocomposites for possible applications as wound dressing materials. *Mater. Sci. Eng. C* **2016**, *65*, 408–418.
- (49) Jagathesan, G.; Rajiv, P. Biosynthesis and characterization of iron oxide nanoparticles using Eichhornia crassipes leaf extract and assessing their antibacterial activity. *Biocatal. Agric. Biotechnol.* **2018**, *13*, 90–94.
- (50) Yuan, X.; Han, L.; Fu, P.; Zeng, H.; Lv, C.; Chang, W.; Runyon, R. S.; Ishii, M.; Han, L.; Liu, K.; et al. Cinnamaldehyde accelerates wound healing by promoting angiogenesis via up-regulation of PI3K and MAPK signaling pathways. *Lab. Invest.* **2018**, *98* (6), 783–798.
- (51) Huang, C. C. High-frequency attenuation and backscatter measurements of rat blood between 30 and 60 MHz. *Phys. Med. Biol.* **2010**, *55* (19), 5801–5815.
- (52) Huang, C. C.; Chen, R.; Tsui, P. H.; Zhou, Q.; Humayun, M. S.; Shung, K. K. Measurements of attenuation coefficient for evaluating the hardness of a cataract lens by a high-frequency ultrasonic needle transducer. *Phys. Med. Biol.* **2009**, *54* (19), 5981–5994.
- (53) Chang, C. C.; Chen, P. Y.; Huang, H.; Huang, C. C. In Vivo Visualization of Vasculature in Adult Zebrafish by Using High-Frequency Ultrafast Ultrasound Imaging. *IEEE Trans Biomed Eng.* **2019**, *66* (6), 1742–1751.
- (54) Lee, S. L. C.; Rouhi, P.; Jensen, L. D.; Zhang, D.; Ji, H.; Hauptmann, G.; Ingham, P.; Cao, Y. Hypoxia-induced pathological angiogenesis mediates tumor cell dissemination, invasion, and metastasis in a zebrafish tumor model. *Proc. Natl. Acad. Sci. U.S.A.* **2009**, *106* (46), 19485–19490.
- (55) Chen, Q.; Jin, T.; Qi, W.; Mo, X.; Xi, L. Label-free photoacoustic imaging of the cardio-cerebrovascular development in the embryonic zebrafish. *Biomed. Opt. Express* **2017**, *8* (4), 2359–2367.